Hindawi
International Journal of Photoenergy
Volume 2023, Article ID 6204891, 17 pages
https://doi.org/10.1155/2023/6204891

Research Article

Design and Performance Enhancement of a GaAs-Based Homojunction Solar Cell Using $Ga_{0.5}In_{0.5}P$ as a Back Surface Field (BSF): A Simulation Approach

Cedrik Fotcha Kamdem, Ariel Teyou Ngoupo, François Xavier Abomo Abega, Aimé Magloire Ntouga Abena, and Jean-Marie Bienvenu Ndjaka

University of Yaoundé 1, Faculty of Science, Department of Physics, P.O. Box: 812, Yaoundé, Cameroon

Correspondence should be addressed to Ariel Teyou Ngoupo; arielteyou@yahoo.fr

Received 17 March 2023; Revised 21 May 2023; Accepted 26 May 2023; Published 14 June 2023

Academic Editor: Fayaz Hussain

Copyright © 2023 Cedrik Fotcha Kamdem et al. This is an open access article distributed under the Creative Commons Attribution License, which permits unrestricted use, distribution, and reproduction in any medium, provided the original work is properly cited.

The GaAs semiconductor is a solar energy promising material for photovoltaic applications due to its good optical and electronic properties. In this work, a homojunction GaAs solar cell with $Al_xGa_{1-x}As$ and $Ga_yIn_{1-y}P$ solar energy materials as window and back surface field (BSF) layers, respectively, was simulated and investigated using SCAPS-1D software. The performance of the GaAs-based solar cell is evaluated for different proportions of x and y, which allowed us to obtain the values of 0.8 and 0.5 for x and y, respectively, as the best values for high performance. We then continued the optimization by taking into account some parameters of the solar cell, such as thickness, doping, and bulk defect density of the p-GaAs base, n-GaAs emitter, and $Ga_{0.5}In_{0.5}P$ BSF layer. Solar cell efficiency increases with emitter thickness, but the recombination phenomenon is more pronounced than that of electron-hole pair generation in the case of a thicker base. The effect of variation in the work function of the back contact has also been studied, and the best performance is for a platinum (Pt) electrode. The optimized GaAs-based solar cell achieves a power conversion efficiency of 35.44% ($J_{SC} = 31.52\,mA/cm^2$, $V_{OC} = 1.26\,V$, FF = 89.14%) and a temperature coefficient of -0.036%/°C. These simulation results provide insight into the various ways to improve the efficiency of GaAs-based solar cells.

1. Introduction

Nowadays, climate change is a real challenge for the society which, paradoxically, continues to increase its energy needs. Due to the limited lifespan of fossil fuels, scientific communities are looking for reliable, cost-effective, and environmentally friendly energy resources [1, 2]. Renewable energy is proving to be an essential asset in solving at least some of these problems. To this end, solar energy can be used as an efficient resource to produce usable electrical energy [3, 4]. Solar energy is the most abundant, clean, nonpolluting, and inexhaustible form of energy found in nature [5, 6]. and solar photovoltaic is dominated by silicon solar energy materials.

The GaAs semiconductor is the most widely used solar energy material in photovoltaic cells for space applications [7] because of its high efficiency due to its direct bandgap of 1.42 eV [8], high carrier mobility, absorption coefficient similar to silicon, and low degradation in the face of space irradiation [6, 9]. However, the problems of surface recombination are hindering the development of this technology, which is why the efficiency achieved for the first solar cells was about 10% [10, 11]. These problems were partially solved by growing an $Al_xGa_{1-x}As$ layer on the front surface of the device. This layer acts as a window layer [12]. Similarly, as a window layer in the device, the semiconductor materials GaInP [13], ZnSe [14], and AlInP [15] can be used. The back contact of a solar cell is also the site of charge recombination processes. The recently simulated performance of GaAs-based solar cells is 28.8 ± 0.9% [16], which is close to the 27.8% efficiency obtained in the laboratory

[17]. This performance is still below the Shockley-Queisser limit for this type of solar energy material. The improvement of this performance is therefore a focus of the research community and is becoming a central issue in the field of GaAs-based solar cells.

The main objective in GaAs-based solar cells is to reduce the surface recombination phenomena observed both at the top, i.e., the front surface, and at the bottom, i.e., the back contact of the cell. In GaAs-based solar cells, the insertion of a window layer and a back surface field (BSF) layer on the front and back surfaces, respectively, is essential to reduce recombination processes. The presence of an integrated electric field on the back surface, due to the presence of the BSF layer, significantly improves the performance of solar cells [18, 19]. For this purpose, the AlGaAs/GaAs(BSF), ZnS/GaAs(BSF), and $Al_{0.8}Ga_{0.2}As/(Al_{0.7}Ga_{0.3})_{0.5}In_{0.5}P$(BSF) window layer/BSF pairs were designed by Abderrezek et al. [18], Najat and Benmoussa [19], and Saif et al. [20], respectively, to reduce the surface recombination phenomena in GaAs-based solar cells. In this work, we will use the $Al_xGa_{1-x}As$ window layer and the $Ga_yIn_{1-y}P$ BSF layer. To the best of our knowledge, a study of the combination of these two layers in GaAs-based solar cells has not yet been done. It is very difficult to experimentally optimize solar cell structures due to their complex implementation, high cost, and manufacturing time. To reduce the time and cost of their implementation, numerical simulations are generally used. Numerical modeling and simulation of GaAs-based solar cell configurations have been proposed [13, 14, 16, 18, 19] to optimize and understand the main physical phenomena involved in these cells. In this work, we optimize the GaAs-based solar cell reported by Kamdem et al. [16], where we incorporate the $Ga_yIn_{1-y}P$ solar energy material as a BSF layer as mentioned above. Using the SCAPS-1D simulation software [21, 22], we will simulate the simultaneous influence of the x and y proportions on the performance of the GaAs-based solar cell. The output electrical characteristics of the GaAs-based solar cell are also investigated for different thicknesses, doping, and bulk defect densities of the emitter layer, base, and BSF layer.

2. Method and Solar Cell Structure

2.1. Simulation Software. The numerical simulations in this work are performed using the solar cell capacitance simulator in one dimension (SCAPS-1D) software, version 3.3.07, originally designed for CdTe and CIGS polycrystalline thin film solar cells. This one-dimensional solar cell simulation program has been developed at the Department of Electronics and Information Systems (ELIS) of the University of Ghent in Belgium [23]. It was made available to researchers in the photovoltaic community in 1998, after the Second World Photovoltaic Conference in Vienna [24]. SCAPS-1D is organized into several panels where the user defines parameters and where the results are displayed. Operating points such as temperature, thickness, voltage, frequency, and illumination, as well as a list of calculation actions to be performed (I-V, C-V, C-f, Q(λ)), can also be defined by the user [25]. The operating parameters in each calculation (V, f, or λ) are varied within the specified range, while all other parameters have the value specified at the operating point [26]. In order to obtain the performance of the simulated solar cell, SCAPS-1D solves the fundamental semiconductor equations [27]: Poisson's equation (Equation (1)) and continuity equations for electrons and holes (Equations (2a), (2b)). The transport equations for electrons and holes are given by Equations (3a) and (3b), respectively.

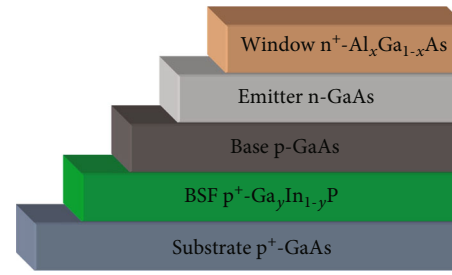

Figure 1: Basic structure of the simulated GaAs-based homojunction solar cell.

$$\frac{\partial^2\varphi(x)}{\partial x^2} = \frac{q}{\varepsilon_{sc}}\left[N_D^+(x) - N_A^-(x) + P(x) - n(x) + \rho_p - \rho_n\right], \tag{1}$$

where φ, q, ε_{sc}, N_D^+, N_A^-, ρ_p, and ρ_n are, respectively, the electrostatic potential, the electric charge, the permittivity of the semiconductor, the ionized donor density, the ionized acceptor density, the hole distribution, and the electron distribution.

$$-\frac{1}{q}\frac{dJ_n(x)}{dx} - G(x) + U_R(x) = 0, \tag{2a}$$

$$-\frac{1}{q}\frac{dJ_p(x)}{dx} + G(x) - U_R(x) = 0, \tag{2b}$$

where G is the optical generation rate ($cm^{-3}.s^{-1}$) and U_R is the recombination rate ($cm^{-3}.s^{-1}$).

$$J_n = -D_n\frac{dn}{dx} + \mu_n n\left(\frac{d\varphi}{dx}\right), \tag{3a}$$

$$J_p = -D_p\frac{dp}{dx} - \mu_p p\left(\frac{d\varphi}{dx}\right), \tag{3b}$$

where J_n and J_p are the current densities of electrons and holes, respectively.

SCAPS-1D uses the Newton-Raphson approach and the Gummel approach for the numerical solution of these fundamental equations.

2.2. Solar Cell Structure and SCAPS-1D Simulation Parameters. The choice of materials to design the solar cell plays an important role in the photogeneration efficiency. Figure 1 shows the schematic structure of the GaAs-based solar cell proposed in this work, where zinc (Zn) is a front contact and molybdenum (Mo) is a back contact; the $Al_xGa_{1-x}As$ layer acts as a window layer; the p-GaAs active

Table 1: SCAPS input material parameters.

	Solar energy materials				
	Window	Emitter	Base	BSF	Substrate
Reference	[16]	[16]	[16]	[28]	[16]
Parameters	n^+-$Al_xGa_{1-x}As$	n-GaAs	p-GaAs	p-$Ga_yIn_{1-y}P$	p^+-GaAs
Thickness (μm)	0.02	0.10	2.00	0.02	0.50
Gap energy (eV)	Varied (2.09 [29])	1.424	1.424	Varied (1.805 [30])	1.424
Electronic affinity (eV)	Varied (3.74 [29])	4.07	4.07	Varied (4.09 [30])	4.07
Dielectric permeability (relative)	10.6	12.9	12.9	11.8	12.9
Density of effective states in the BC (cm^{-3})	8×10^{19}	1×10^{17}	1×10^{17}	6.5×10^{17}	1×10^{17}
Density of effective states in the BV (cm^{-3})	1×10^{19}	1×10^{19}	1×10^{19}	1.45×10^{19}	1×10^{19}
Thermal velocity of electrons (cm/s)	2.3×10^5	4.4×10^5	4.4×10^5	2.3×10^5	4.4×10^5
Thermal velocity of the holes (cm/s)	1.4×10^5	1×10^5	1×10^5	1.4×10^5	1×10^5
Electron mobility (cm^2/V.s)	212	8500	8500	717.7	8500
Hole mobility (cm^2/V.s)	126	370	370	40	370
Donor density ND (cm^{-3})	2×10^{18}	2×10^{18}	0	0	0
Acceptor density NA (cm^{-3})	0	0	2×10^{17}	2×10^{18}	2×10^{18}
Absorption coefficient	SCAPS	SCAPS	SCAPS	SCAPS	SCAPS

Table 2: Electronic properties of $Al_xGa_{1-x}As$ and $Ga_yIn_{1-y}P$ materials at 300 K.

Parameter	Solar energy materials	
	$Al_xGa_{1-x}As$ [34]	$Ga_yIn_{1-y}P$ [28]
Gap energy Eg (eV)	$1.424 + 1.247x$ for $x \le 0.45$ $1.9 + 0.125x + 0.143x^2$ for $0.45 < x < 1$	$1.3399 + 0.69y + 0.48y^2$
Electronic affinity χ (eV)	$4.07 - 1.1x$ for $x \le 0.45$ $3.64 - 0.14x$ for $0.45 < x < 1$	$4.38 - 0.58y$

layer is between the n-GaAs emitter and the $Ga_yIn_{1-y}P$ back surface field (BSF) layer. The p^+-GaAs layer is the substrate on which cell growth occurs; it plays the roles of support and protection. $Ga_yIn_{1-y}P$ semiconductor material is a promising candidate for a BSF layer because its electronic properties (gap and electronic affinity) can be modulated by the gallium. Its gap varies between 1.344 eV (InP) and 2.26 eV (GaP) [28]. The parameters used in this simulation are based on values from literature theory [16, 28–30] and, in some cases, reasonable estimates; they are listed in Table 1. To reflect the experimental quantum efficiency data, the reflectivities of the front and rear contacts are set to 0.1 and 0.9, respectively. The default operating temperature is set to 300 K. The illumination spectrum is set to the AM1.5G standard. Simulations are performed with zero series resistance and infinite shunt resistance.

3. Results and Discussion

The basic solar cell structure studied in this work is that from the work of Kamdem et al. [16], in which we introduce a back surface field (BSF) layer as shown in Figure 1. We will first study the effect of the x and y proportions of aluminum (Al) in the window layer ($Al_xGa_{1-x}As$) and gallium (Ga) in the BSF layer ($Ga_yIn_{1-y}P$) on the performance of the solar cell. Then, we will proceed to improve its performance by studying the influence of thickness, doping, and bulk defect density on the emitter layer (n-GaAs), base (p-GaAs), and BSF layer ($Ga_yIn_{1-y}P$). Finally, the influence of the back contact metal work function is studied, and the effect of the operating temperature of the optimized GaAs-based solar cell is presented.

3.1. Influence of the Proportions x and y on the Solar Cell Electrical Parameters. Changing the electronic properties of a solar energy material affects the device's performance. A common best window layer is susceptible to a wide bandgap for efficient solar cells. Then, it is important to choose the correct values of x and y for compound semiconductors to satisfy the lattice matching between different alloys [31, 32]. The refractive index (n) and extinction coefficient (k) of the compound semiconductor vary with its mole fraction [33]. Table 2 shows the evolution of the bandgap and the electron affinity as a function of the proportions x and y of aluminum in the window layer and gallium in the BSF layer, respectively [28, 34]. From these equations, we first

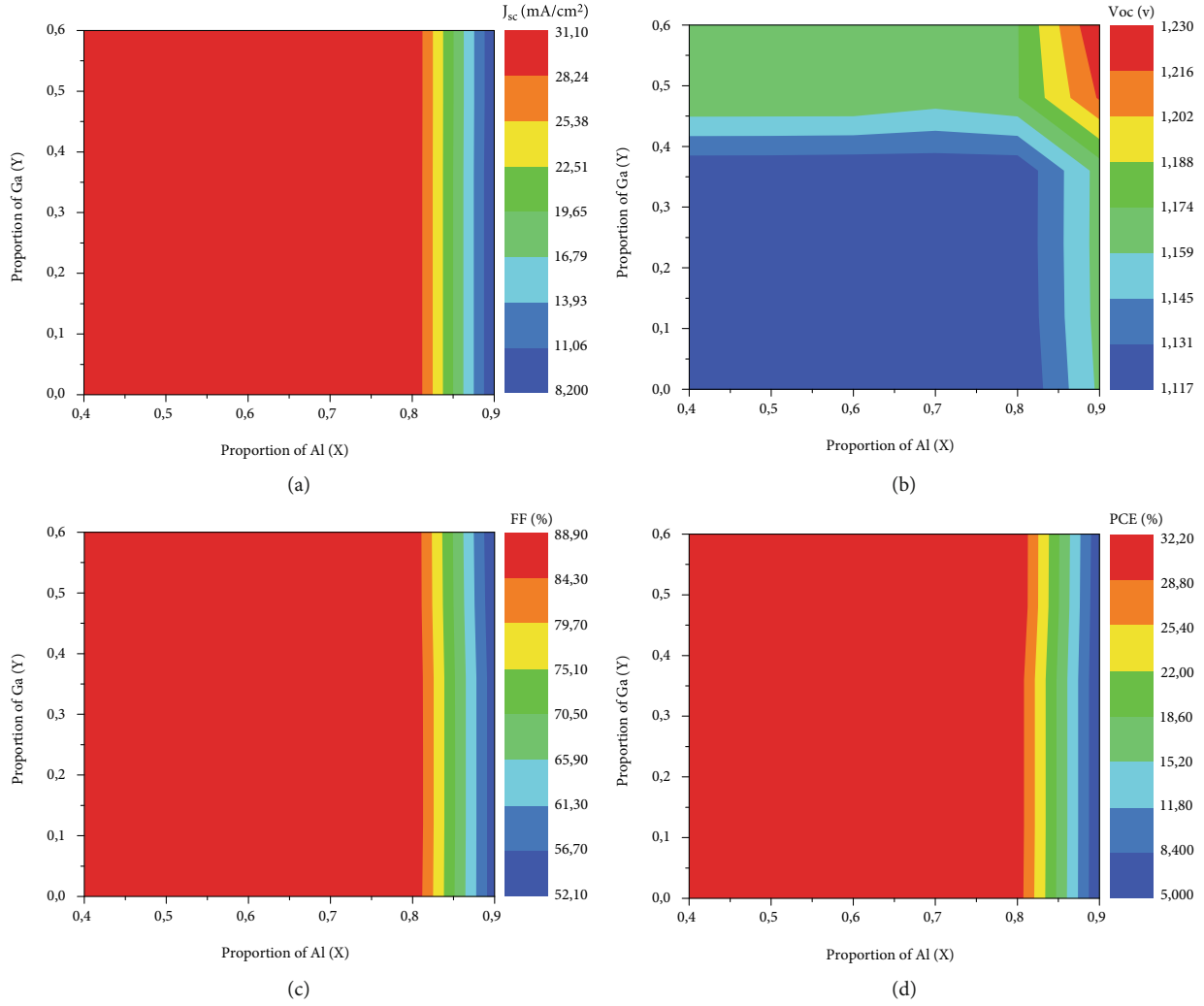

Figure 2: Variation of the electrical parameters as a function of the x and y proportions: (a) J_{SC}, (b) V_{OC}, (c) FF, and (d) PCE.

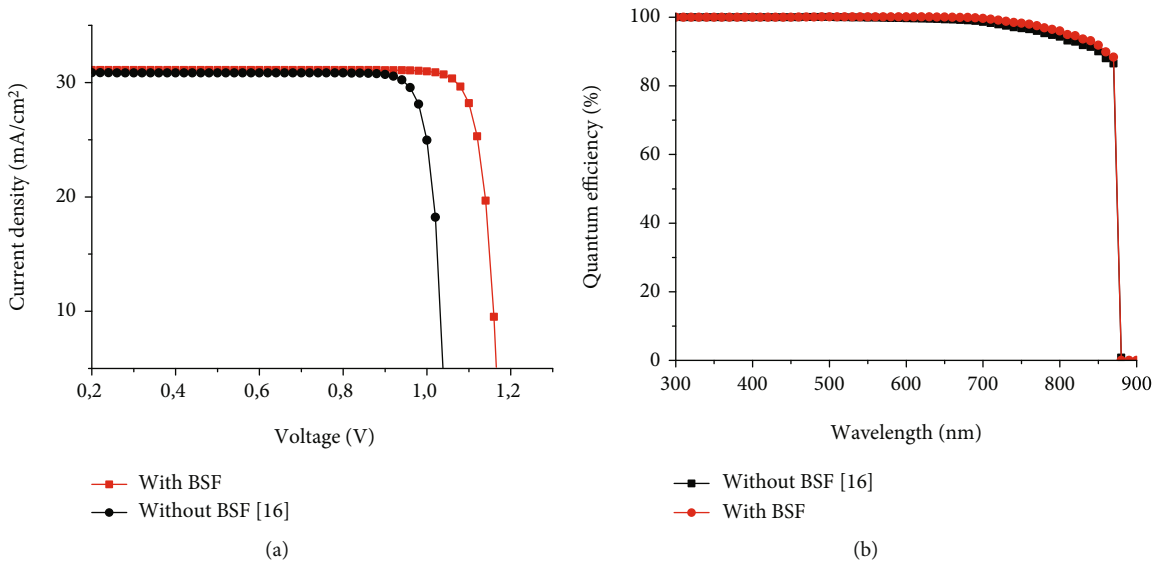

Figure 3: (a) Current-voltage (J-V) characteristics and (b) quantum efficiency of the GaAs-based solar cell without and with $Ga_{0.5}In_{0.5}P$ BSF layer.

Table 3: Comparison of the GaAs-based solar cell electrical parameters without and with $Ga_{0.5}In_{0.5}P$ BSF layer.

Solar cell	Electrical parameters			
	J_{SC} (mA/cm^2)	V_{OC} (V)	FF (%)	PCE (%)
Without BSF [16]	30.87	1.035	85.68	27.37
With $Ga_{0.5}In_{0.5}P$ BSF layer	31.09	1.178	88.28	32.19

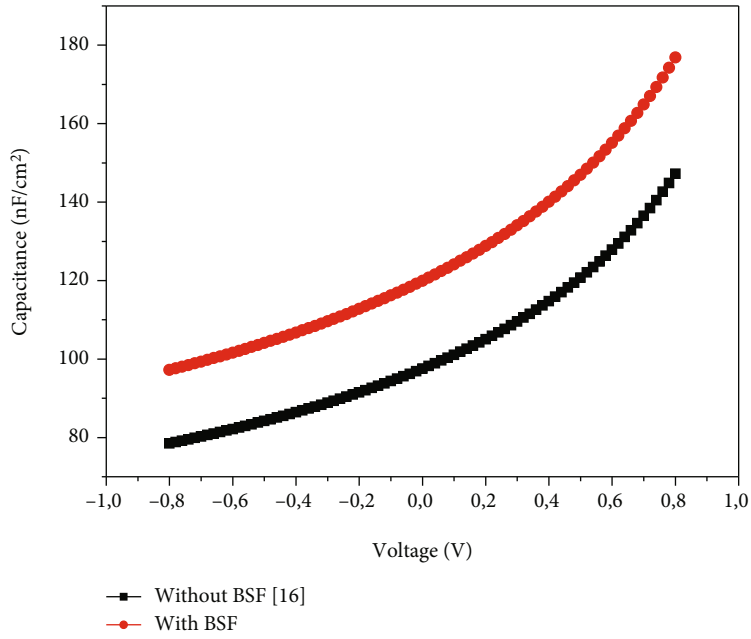

Figure 4: Capacitance-voltage (C-V) characteristics of the GaAs-based solar cell without and with $Ga_{0.5}In_{0.5}P$ BSF layer.

calculated the corresponding values of gap energy and electronic affinity for each x and y pair considered in this work. Then, for each selected pair (x, y), we enter into the SCAPS-1D software, the corresponding values of the gap energy, and the electronic affinity of the $Al_xGa_{1-x}As$ window layer and the $Ga_yIn_{1-y}P$ BSF layer. Finally, using the "calculate: single shot" function in the SCAPS-1D action panel, the simulations are performed for each pair (x, y), and each result of the obtained electrical parameters (J_{SC}, V_{OC}, FF, and PCE) is recorded in a double entry table, from which the contour plots in Figure 2 are made. Figure 2 allows us to determine the (x, y) pair that achieves the optimal performance of the GaAs-based solar cell.

In Figure 2(d), we observe that the power conversion efficiency (PCE) of the solar cell gradually increases with the fraction of x up to its maximum value ($x = 0.8$) and then decreases, regardless of the fraction of y. Moreover, for $x = 0.8$, there is a better compromise between AlGaAs and GaAs semiconductors [35]; this is also in agreement with the work of Salem et al. [36]. The short circuit current density J_{SC} (Figure 2(a)) and the fill factor FF (Figure 2(c)) follow the same trend as the solar cell efficiency. This is understandable because there is a proportional relationship between them (Equation (4)). The open circuit voltage V_{OC} (Figure 2(b)), on the other hand, varies very little with the proportions x and y. According to the work of Olson et al. [37], $Ga_yIn_{1-y}P$ forms a good interface with the GaAs material for a Ga mole fraction equal to 0.5, and the resistivity of the $Ga_{0.5}In_{0.5}P$ semiconductor is maximal [34]. We also observe that for this fraction, the electrical parameters (J_{SC}, FF, and PCE) in Figure 2 are optimal for $x \leq 0.8$. Thus, the $Al_{0.8}Ga_{0.2}As$ and $Ga_{0.5}In_{0.5}P$ compounds used as window and BSF layers in Figure 1 lead to a better performance of the GaAs-based solar cell. The values $x = 0.8$ and $y = 0.5$ are in agreement with the values used by Bourbaba et al. in their work [13].

$$\text{PCE} = \frac{J_{sc} \times V_{oc} \times \text{FF}}{P_{in}}. \quad (4)$$

3.2. Comparison of a Cell without and with $Ga_{0.5}In_{0.5}P$ BSF Layer. Using the solar cell structure proposed in Figure 1, the parameters listed in Table 1, and the $Ga_{0.5}In_{0.5}P$ BSF layer, Figures 3(a) and 3(b) show the J-V characteristics and quantum efficiency (QE(λ)) curves of the GaAs-based solar cell without and with the BSF layer, respectively. As we can see from Figure 3(a), the addition of the $Ga_{0.5}In_{0.5}P$ BSF layer in the solar cell has a remarkable influence on its performance (Table 3). There is a significant improvement in the short circuit current density (J_{SC}) and open circuit

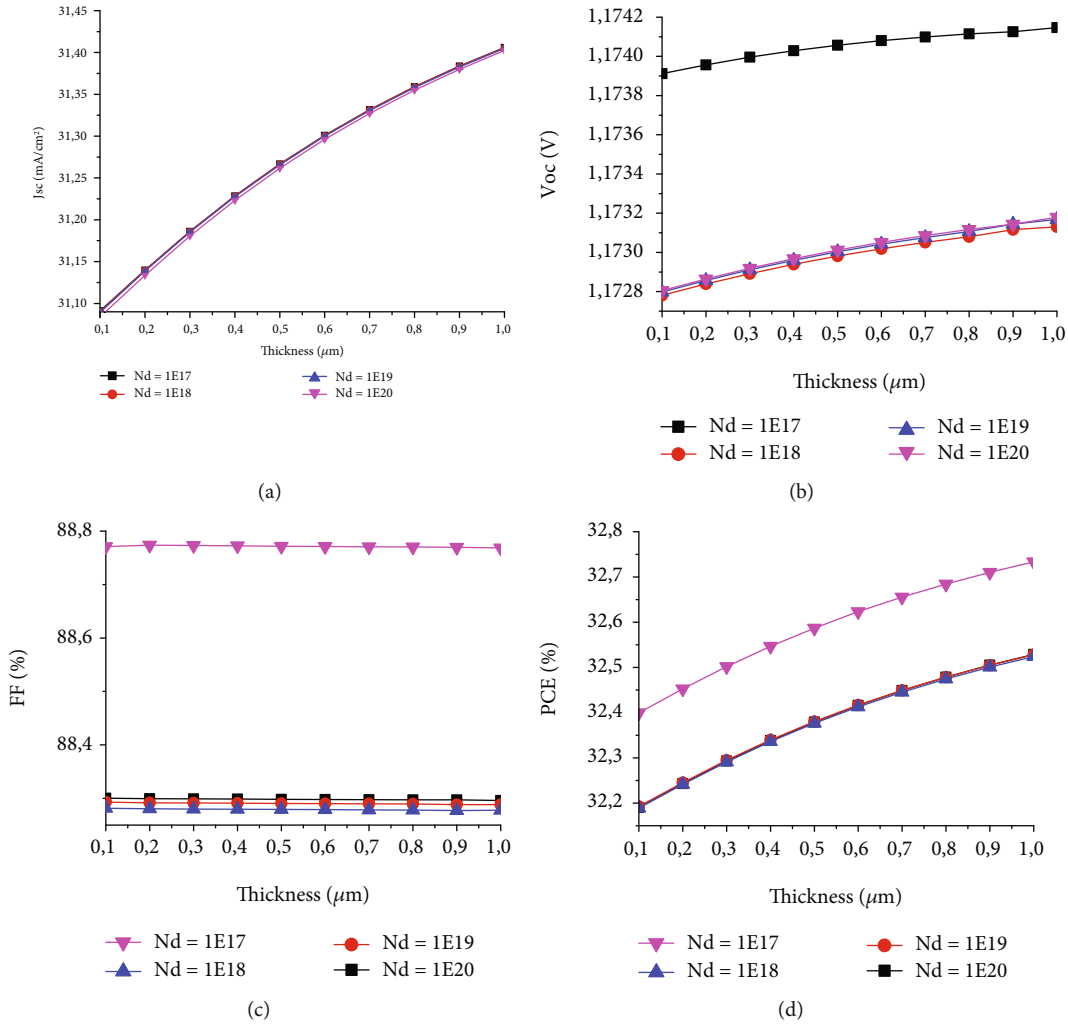

Figure 5: Variation of photovoltaic parameters as a function of n-GaAs emitter layer thickness and carrier concentration: (a) J_{SC}, (b) V_{OC}, (c) FF, and (d) efficiency (PCE).

voltage (V_{OC}), as well as the power conversion efficiency (PCE), of the solar cell due to the additional absorption of photons with wavelengths between 700 nm and 900 nm in the case of the solar cell with a BSF layer (Figure 3(b)). These improvements are also reflected in the fact that the presence of the back surface field (BSF) creates a potential barrier on the backside of the solar cell in order to ensure passivation. This potential barrier, induced by the difference in doping level between the GaAs base and the $Ga_{0.5}In_{0.5}P$ BSF layer, tends to confine the minority carriers in the GaAs base due to the presence of an additional internal electric field in the cell. These minority carriers are thus kept away from the backside where they can be recombined; consequently, they are pushed towards the space charge region for better collection. These observations are in agreement with the literature [38, 39].

Figure 4 shows the evolution of the capacitance-voltage (C-V) characteristic for the GaAs-based solar cell without and with BSF. The diffusion voltage (V_d) and the charge carrier density (N_a) can be extracted from the C-V measurements according to the Mott-Schottky analysis method (Equation (5)) used in conventional devices containing *p-n* junctions. It is observed that the addition of the BSF layer favors the increase of the C-V curve due to the increase of the charge carrier density (N_a) in the space charge region (SCR) of the solar cell, from which a better performance is achieved (Table 3).

$$\frac{1}{C^2} = \frac{2\mathcal{E}_0\mathcal{E}}{qN_a}(V_d - V). \tag{5}$$

3.3. Influence of n-GaAs Emitter Layer on Electrical Parameters

3.3.1. Thickness and Doping of the n-GaAs Layer. In the GaAs-based solar cell, the most important layers are the emitter and the base, since they form the metallurgical interface and play the role of active layers in which the majority of photons with an energy greater than or equal to that of the bandgap of the semiconductor material are absorbed. To obtain interesting performances, it is therefore important

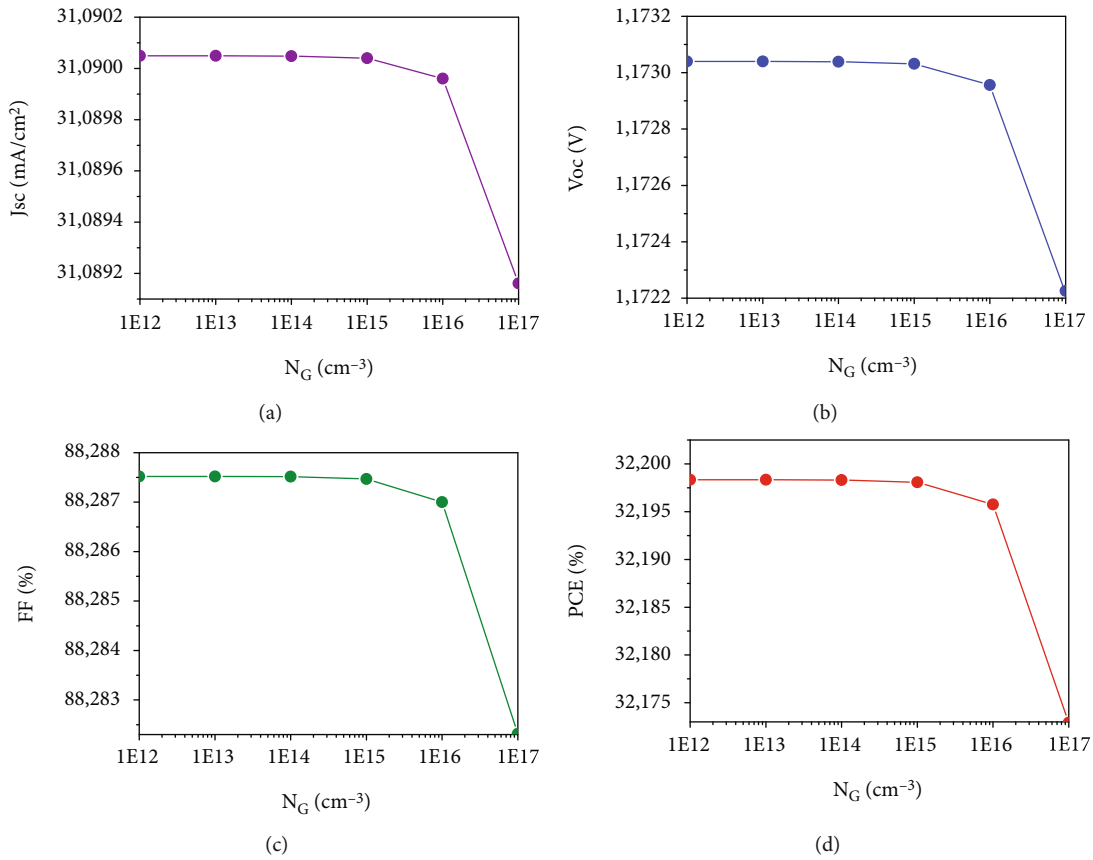

FIGURE 6: Variation of electrical parameters of the GaAs-based solar cell as a function of n-GaAs emitter defect density: (a) J_{SC}, (b) V_{OC}, (c) FF, and (d) efficiency (PCE).

to control the thickness [40] and doping of each layer constituting the solar cell. In this subsection, we will evaluate the variations of the electrical parameters of the GaAs-based solar cell as a function of the thickness and doping of the n-GaAs emitter layer, by varying them from 0.1 μm to 1 μm and from 10^{17} cm^{-3} to 10^{20} cm^{-3}, respectively. Figure 5 shows the results of the numerical simulation.

From Figure 5, we can see that for doping between 10^{17} cm^{-3} and 10^{20} cm^{-3}, the electrical parameters J_{SC} (Figure 5(a)), V_{OC} (Figure 5(b)), and PCE (Figure 5(d)) increase with the thickness of the n-GaAs emitter; this is explained by the fact that as the thickness of the n-GaAs emitter increases, the number of absorbed photons increases and thus a large number of electron-hole pairs are generated. This increase in the generation rate (G) of the electron-hole pairs mainly increases the J_{SC} (Equation (6) [41]), which in turn induces the increase in the V_{OC} through Equation (7) [42]. Moreover, increasing the thickness of the n-GaAs emitter reduces the recombination phenomenon (J_0) at the level of the front contact of the solar cell.

The fill factor (FF) (Figure 5(c)) varies very little with the doping and remains unchanged with the increasing thickness of the n-GaAs emitter. Except for J_{SC}, V_{OC}, and PCE also vary with the doping and reach their maximum at $N_D = 10^{17}$ cm^{-3}. The low values of V_{OC} and PCE at too high doping can be explained by the fact that this process affects the mobility of the free carriers, limiting their collection by the front contact of the solar cell; this is in agreement with the literature since the mobility of the emitter carriers decreases at high doping [43]. The efficiency increases with the n-GaAs emitter thickness and starts to vary very slightly beyond 0.7 μm; it is also maximal for doping of 10^{17} cm^{-3}. This leads us to choose the values 0.7 μm and 10^{17} cm^{-3} as the thickness and doping of the n-GaAs emitter layer, respectively.

$$J_{ph} = J_{SC} = q \bullet G \bullet \left(L_n + W + L_p\right), \tag{6}$$

$$V_{OC} = n \bullet \frac{\mathrm{kT}}{\mathrm{q}} \bullet \mathrm{In}\left(\frac{J_{sc}}{J_0} + 1\right). \tag{7}$$

3.3.2. Density of Defects in the n-GaAs Emitter Layer. Defect densities are also considered limiting factors for solar cell performance. These defects affect the recombination of carriers, their lifetime, and their mobility [44]. In our simulations, we have used Gaussian-type defects, characterized by their concentration N_G, to evaluate their effects on the electrical parameters of the GaAs-based solar cell. They vary from 10^{12} cm^{-3} to 10^{17} cm^{-3}, and Figure 6 illustrates their effects on J_{SC} (Figure 6(a)), V_{OC} (Figure 6(b)), FF (Figure 6(c)), and Efficiency (PCE) (Figure 6(d)). It can be seen that the performance of the simulated GaAs-based solar cell remains unchanged

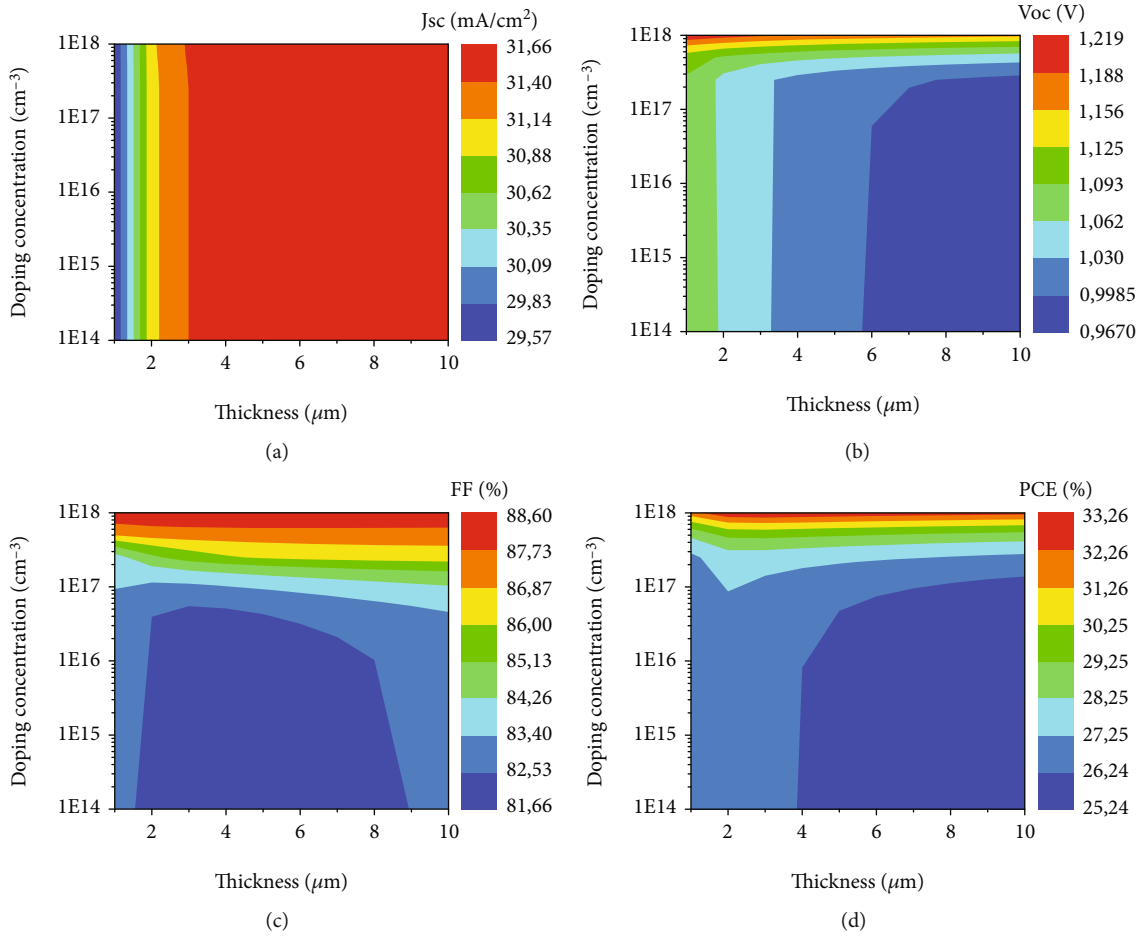

Figure 7: Variation of GaAs-based solar cell performance with thickness and acceptor concentration of the p-GaAs layer: (a) J_{SC}, (b) V_{OC}, (c) FF, and (d) PCE.

when the defect density is less than 10^{15} cm^{-3}; and beyond this concentration, the electrical parameters (J_{SC} (Figure 6(a)), V_{OC} (Figure 6(b)), FF (Figure 6(c)), and PCE) (Figure 6(d)) decrease drastically. Increasing the number of defects ($N_G > 10^{15}$ cm^{-3}) in the n-GaAs emitter introduces new recombination centers, which increase the recombination of photogenerated carriers in the solar cell, thus causing a decrease in the electrical parameters (J_{SC}, V_{OC}, FF, and PCE). For our further simulations, we choose the value $N_G = 10^{15}$ cm^{-3} as the defect density in the n-GaAs emitter layer.

3.4. Influence of p-GaAs Active Layer on Electrical Parameters

3.4.1. Thickness and Doping of the p-GaAs Layer. In a solar cell, the photovoltaic conversion usually takes place at the base. Figure 7 shows the variations of the electrical parameters (J_{SC}, V_{OC}, FF, and PCE) of the GaAs-based solar cell as a function of the thickness and doping of the p-GaAs base, taken in the ranges (1 μm, 10 μm) and (10^{14} cm^{-3}, 10^{18} cm^{-3}), respectively. It is observed that these electrical parameters are affected by varying both the thickness and the doping of the p-GaAs base layer.

We observe that for a doping greater than 10^{16} cm^{-3}, the open circuit voltage (Figure 7(b)), the fill factor (Figure 7(c)), and the efficiency (Figure 7(d)) increase with doping, regardless of the thickness of the p-GaAs base and reach their maximum for a doping around 10^{18} cm^{-3}. For a given thickness of the p-GaAs base, however, the short-circuit current density (Figure 7(a)) is independent of doping. We also note that the increase in the p-GaAs layer thickness is accompanied by a progressive decrease in the V_{OC} (Figure 7(b)) on the one hand and, on the other hand, an increase in J_{SC} (Figure 7(a)). These observations are in agreement with those reported by other authors [45–47]. The increase in J_{SC} with thickness is due to the increase in the space charge region (SCR) (Equation (6)) and the fact that more photons are absorbed in the p-GaAs substrate when it is thicker. As in the case of the n-GaAs emitter layer, we observe the generation of a larger number of electron-hole pairs. The decrease of the V_{OC} with the thickness of the p-GaAs base can be caused by the increase of the defect density in this layer, which increases the saturation current J_0 and increases the probability of charge carrier recombination [48]. This can be explained by the dependence of V_{OC} on J_0 and the photogenerated current (J_{SC}) given by Equation (7) [42].

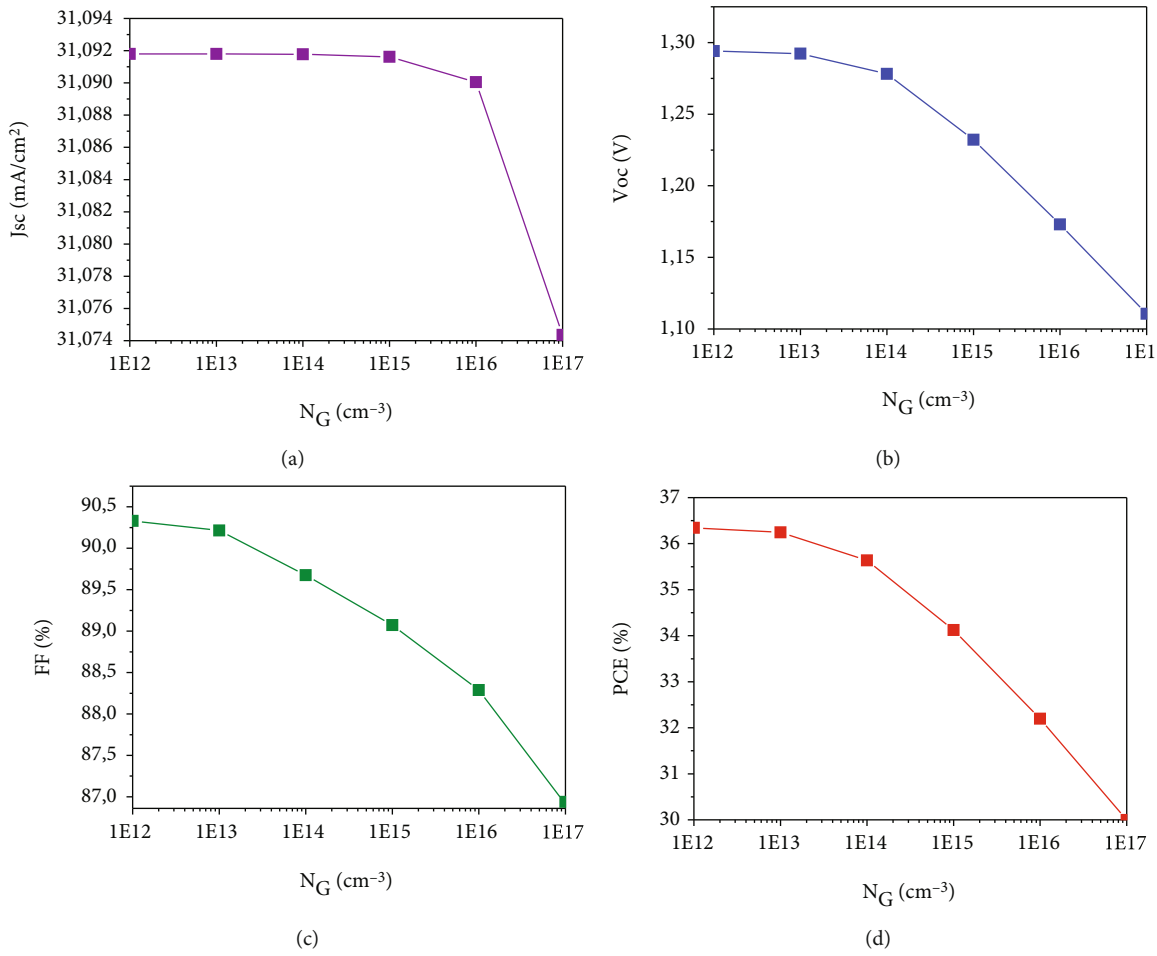

FIGURE 8: Influence of the bulk defect density of the p-GaAs layer on the electrical parameters of the GaAs-based solar cell: (a) J_{SC}, (b) V_{OC}, (c) FF, and (d) PCE.

The recombination phenomenon is more pronounced than the electron-hole pair generation in the case of a thicker base. The efficiency is maximal for a thickness of 2 μm and a doping of 10^{18} cm^{-3} of the p-GaAs layer; this leads us to choose these values as the thickness and doping of the p-GaAs active layer, respectively.

3.4.2. Effect of Defect Density in the p-GaAs Base. We use bulk defects whose energy distribution is of the Gaussian type, characterized by the concentration N_G. To evaluate the effect of these defects on the electrical parameters of the GaAs-based solar cell, we vary their concentration between 10^{12} cm^{-3} and 10^{17} cm^{-3}, and Figure 8 shows the results obtained from the numerical simulation. On the one hand, we find that V_{OC} (Figure 8(b)), FF (Figure 8(c)), and PCE (Figure 8(d)) remain almost unchanged when the bulk defect density of the p-GaAs layer is less than 10^{13} cm^{-3}; this observation is the same for J_{SC} (Figure 8(a)) when the bulk defect density is less than 10^{15} cm^{-3}. On the other hand, V_{OC}, FF, and PCE decrease when the bulk defect density is greater than 10^{13} cm^{-3}; this observation is the same for J_{SC} when this density is greater than 10^{15} cm^{-3}. The increase in the number of volume defects in the base introduces new recombination centers which have the effect of increasing the recombination phenomenon of the photogenerated carriers; this therefore causes a decrease in J_{SC}, V_{OC}, FF, and PCE. For the rest of our simulations, we choose the value of 10^{13} cm^{-3} as the optimal value of the bulk defect density in the p-GaAs base.

3.5. Effect of $Ga_{0.5}In_{0.5}P$ BSF Layer on Cell Performance

3.5.1. Thickness and Bulk Defect Density of the $Ga_{0.5}In_{0.5}P$ Layer. A back surface field (BSF) layer is generally used to reduce the back contact recombination processes and improve the performance of a solar cell [20, 49, 50]. To study the effect of $Ga_{0.5}In_{0.5}P$ BSF film on the electrical parameters of the proposed solar cell (Figure 1), we vary its thickness and bulk defect density between 0.01 μm and 0.07 μm and 10^{14} cm^{-3} and 10^{19} cm^{-3}, respectively, as shown in Figure 9.

It can be seen that the electrical parameters (J_{SC}, V_{OC}, FF, and PCE) are not affected by the variation of the volume defects in the $Ga_{0.5}In_{0.5}P$ BSF layer, regardless of its thickness. On the other hand, for a fixed volume defect density, J_{SC} (Figure 9(a)), V_{OC} (Figure 9(b)), and PCE (Figure 9(d)) increase very slightly with the thickness of the $Ga_{0.5}In_{0.5}P$ BSF layer due to the fact that long-wavelength photons are absorbed and generate a small amount of electron-hole pairs. Furthermore, the back contact recombination rate decreases

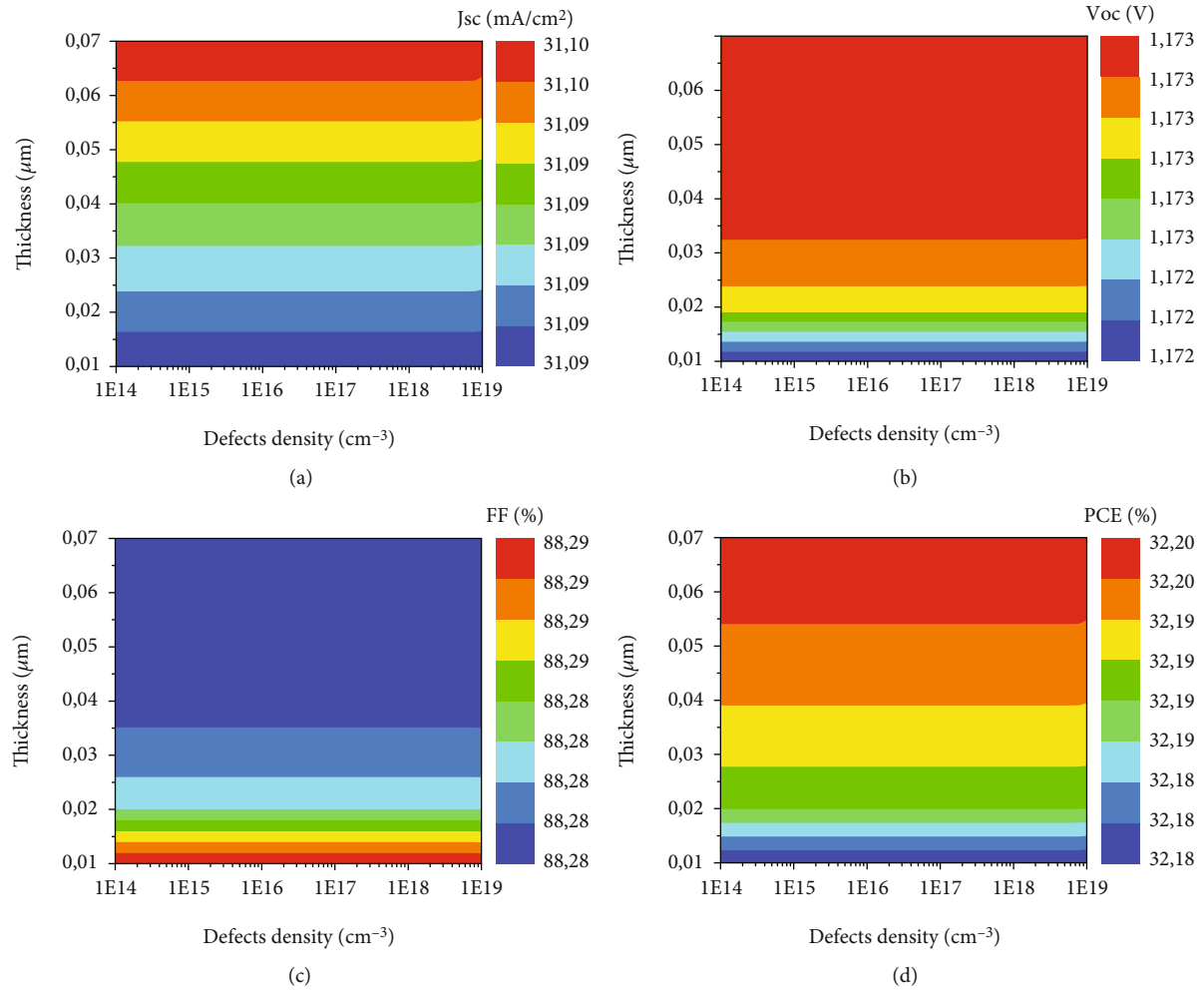

Figure 9: Performance variation of GaAs-based solar cell as a function of thickness and bulk defect density of $Ga_{0.5}In_{0.5}P$ BSF layer: (a) J_{SC}, (b) V_{OC}, (c) FF, and (d) PCE.

with the increasing thickness of the $Ga_{0.5}In_{0.5}P$ BSF layer. These results are in agreement with those performed by Benzetta et al. [51] and Moon et al. [52]. Figure 9(c) shows the evolution of the fill factor, which is opposite to that of the V_{OC}; for a fixed value of the bulk defect density, the FF decreases slightly with increasing thickness of the $Ga_{0.5}In_{0.5}P$ BSF layer; this may be due to the fact that large thicknesses can introduce resistive components that are detrimental to the fill factor [53]. For the remainder of our simulations, we set the thickness of the $Ga_{0.5}In_{0.5}P$ BSF layer to 0.055 μm.

3.5.2. Effect of the Doping Density of the $Ga_{0.5}In_{0.5}P$ BSF Layer. In this subsection, we will focus on the effect of $Ga_{0.5}In_{0.5}P$ BSF layer doping on the electrical parameters of GaAs-based solar cell. To do this, we vary the doping between $10^{16}\,cm^{-3}$ and $10^{19}\,cm^{-3}$, and Figure 10 shows the results obtained from the simulation. We observe that the performance of the solar cell is slightly affected by the variation of the doping of the $Ga_{0.5}In_{0.5}P$ BSF layer. On the one hand, we observe a slight increase in V_{OC} (Figure 10(b)) and efficiency (Figure 10(d)), and on the other hand, we observe a slight decrease in J_{SC} (Figure 10(a)) and FF (Figure 10(c)). The decrease in J_{SC} with the increase in doping may be due to the fact that excessive doping of the $Ga_{0.5}In_{0.5}P$ BSF layer promotes the recombination process of minority carriers before they reach the SCR. The improvement in V_{OC} and PCE is due to the fact that the potential barrier, induced by the difference in doping level between the p-GaAs base and the $Ga_{0.5}In_{0.5}P$ layer BSF, tends to confine the minority carriers in the p-GaAs base, thus keeping them away from the backside and pushing them back towards the SCR for better collection. This improves the electron-hole pair generation rate, which increases the power conversion efficiency of the solar cell. The decrease in the fill factor can be attributed to the fact that as the V_{OC} increases, the integrated electric field in the space charge region of the absorber layer decreases [54]. The power conversion efficiency of the solar cell increases slightly and seems to stabilize beyond a doping of $5 \times 10^{18}\,cm^{-3}$ of the $Ga_{0.5}In_{0.5}P$ BSF layer.

3.6. Influence of the Back Contact. Metal contacts play an essential role in the collection of charge carriers from the absorber layer [55]. To investigate the influence of the back

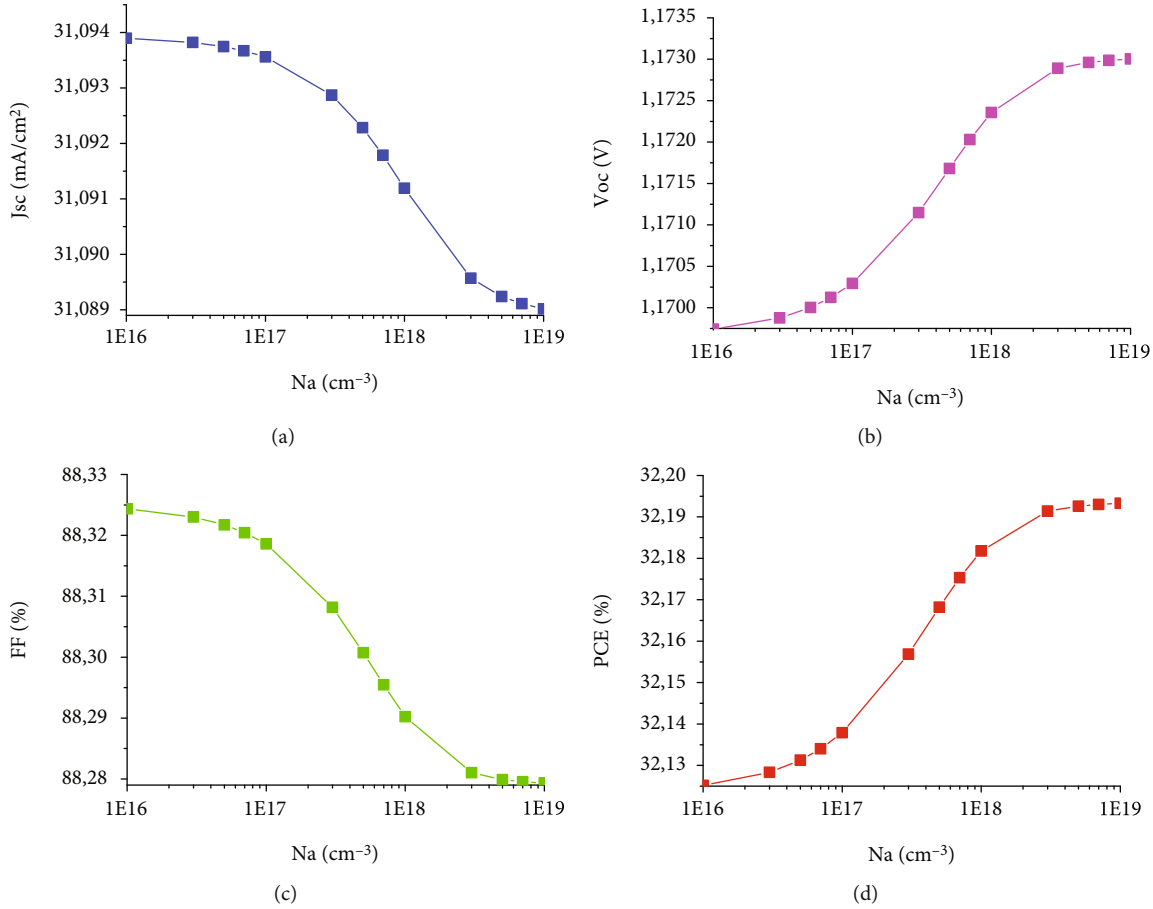

FIGURE 10: Variation of photovoltaic parameters of the GaAs-based solar cell as a function of doping of the $Ga_{0.5}In_{0.5}P$ BSF layer: (a) J_{SC}, (b) V_{OC}, (c) FF, and (d) PCE.

contact work function on the solar cell performance, different metals (Mo, Ni, Au, and Pt) with work functions ranging from 5 eV to 5.93 eV are used. These metals are taken from the work of Michaelson [56] and Hölzl and Schulte [57]. Figure 11 and Table 4 show, respectively, the performance evolution and the synthesis of the electrical parameters of the GaAs-based solar cell for these different metals. In Figure 11, it is observed that the solar cell performance increases with the work function of the back contact; this is due to the decrease in the Schottky barrier height (ϕ_b) (Table 4) for the majority of charge carriers (holes) at the p^+-GaAs/metal interface. Thus, decreasing the Schottky barrier height (ϕ_b) reduces the recombination rate at the back contact and improves the device's performance. The platinum (Pt) electrode exhibits the highest solar cell performance (Table 4) due to its highest work function; these observations are in agreement with the work of other authors, including Thahab et al. [58] in the case of a GaN-based solar cell and Rana et al. [59] in the case of a CZTS-based solar cell.

3.7. Optimized Solar Cell and Comparison of Results. Based on the results obtained in the previous sections, we can determine the GaAs-based solar cell that gives the best performance using the maximum parameters of thickness, doping, and bulk defect density of the different layers studied; these values are summarized in Table 5. Using these values, we compare the J-V characteristics (Figure 12(a)) and the quantum efficiency (Figure 12(b)) of the GaAs-based solar cell without a BSF layer, with a BSF layer, and optimized. From Figure 12(a), we can see that there is a slight and clear improvement in J_{SC} and V_{OC}, respectively, of different structures of the GaAs-based solar cell. The improvement in J_{SC} is mainly due to the absorption of more photons at longer wavelengths (700 nm-900 nm (Figure 12(b)), which generates slightly more electron-hole pairs. The improvement in V_{OC} is due to the reduction of the recombination rate at the back contact due to the presence of the $Ga_{0.5}In_{0.5}P$ BSF layer and the reduction of the Schottky barrier height. Thus, the optimized solar cell achieves a power conversion efficiency of 35.44% ($J_{SC} = 31.52\,mA/cm^2$, $V_{OC} = 1.26\,V$, FF = 89.14%), which is an increase of about 29.5% in efficiency compared to the configuration proposed by Kamdem et al. [16]. In order to compare our results, Table 6 summarizes the values of the electrical parameters of the initial [16] and optimized solar cells, as well as those performed by other authors [16, 18–20, 60].

Figure 13 shows the band structure of the optimized GaAs-based solar cell under AM1.5G illumination. When

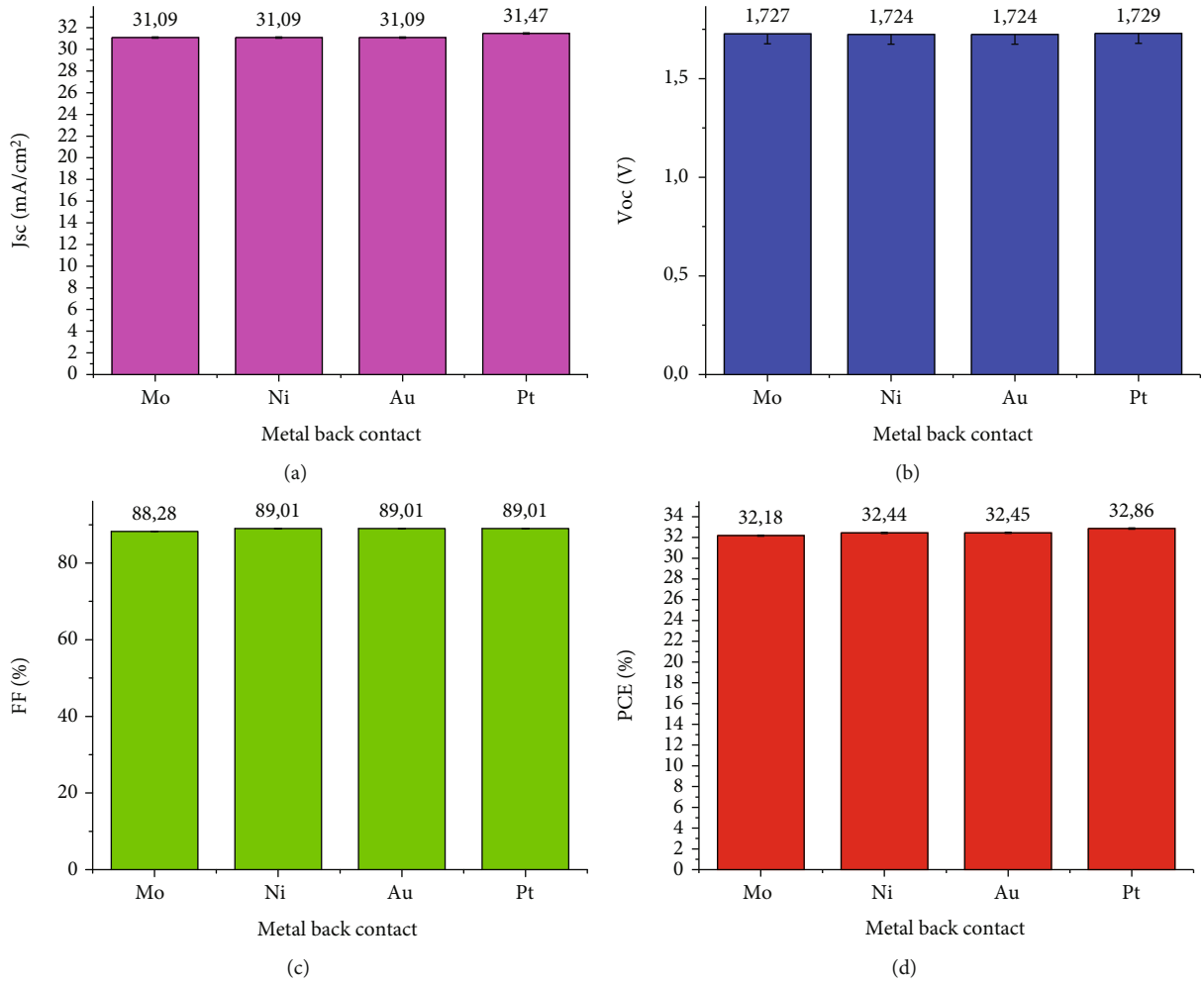

Figure 11: Variation of the electrical parameters of the GaAs-based solar cell as a function of back contact: (a) J_{SC}, (b) V_{OC}, (c) FF, and (d) PCE.

Table 4: Solar cell output parameters for different back contacts.

Rear contact	Electron work function (eV)	$\phi_b = E_g + \chi - \phi_M$	V_{OC} (V)	J_{SC} (mA/cm^2)	FF (%)	PCE (%)
Mo	5.00	0.50	1.727	31.09	88.28	32.18
Ni	5.35	0.15	1.724	31.09	89.01	32.44
Au	5.47	0.03	1.724	31.09	89.01	32.45
Pt	5.93	-0.43	1.129	31.47	89.01	32.86

Table 5: Parameters optimized for this simulation.

Layer	Parameters		
	Thickness (μm)	Doping (cm^{-3})	Bulk defect density (cm^{-3})
Emitter	0.70	10^{17}	10^{15}
Base	2.00	10^{18}	10^{13}
Back surface field	0.55	5×10^{18}	10^{16}

the solar cell is illuminated, the conduction and valence bands of the materials constituting the solar cell are well observed, as well as the Fermi level E_f, which uniquely determines the probability of occupation of the different levels by an electron [47]. In addition to the levels at the bottom of the conduction band E_C and at the top of the valence band E_V, the quasi-Fermi levels F_n for the electrons and F_p for the holes can be observed. These levels are due to the fact that

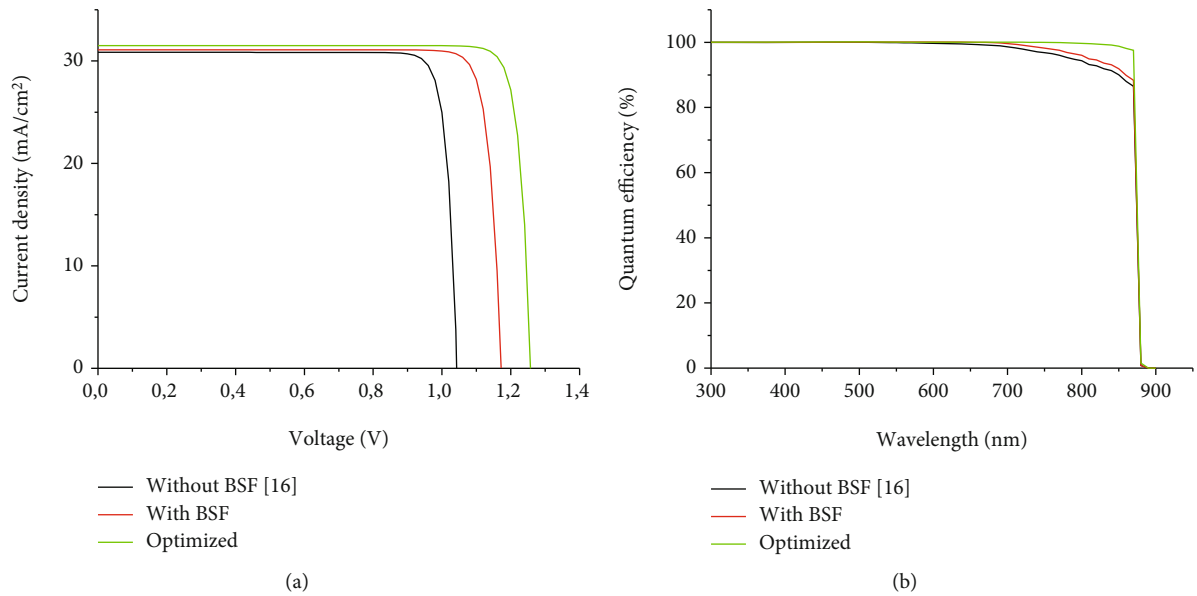

Figure 12: (a) J-V characteristics and (b) quantum efficiency of the GaAs-based solar cell without BSF layer, with BSF layer, and optimized.

Table 6: Comparison of electrical parameters of some GaAs-based solar cells.

Cell structure	Electrical parameters				Reference
	V_{OC} (V)	J_{SC} (mA/cm^2)	FF (%)	PCE (%)	
n^+-$Al_{0.8}Ga_{0.2}As$/n-GaAs/p-GaAs/substrate	1.035	30.87	85.68	27.37	[16]
n^+-AlGaAs/n-GaAs/p-GaAs/p^+-GaAs(BSF)/substrate	1.008	29.50	86.76	25.80	[18]
(MgF_2/ZnS)/n^+-GaAs/p-GaAs/p^+-GaAs(BSF)/substrate	0.980	30.80	86.29	26.80	[19]
p^+-$Al_{0.8}Ga_{0.2}As$/p-GaAs/n-GaAs/n^+-$(Al_{0.7}Ga_{0.3})_{0.5}In_{0.5}P$(BSF)	1.000	52.58	88.54	33.94	[20]
n-InAlGaP/n-GaAs/p-GaAs/GaAs(buffer)/substrate	1.000	34.79	85.00	29.75	[60]
n^+-$Al_{0.8}Ga_{0.2}As$/n-GaAs/p-GaAs/p^+- $Ga_{0.5}In_{0.5}P$(BSF)/substrate	1.260	31.52	89.14	35.44	This work

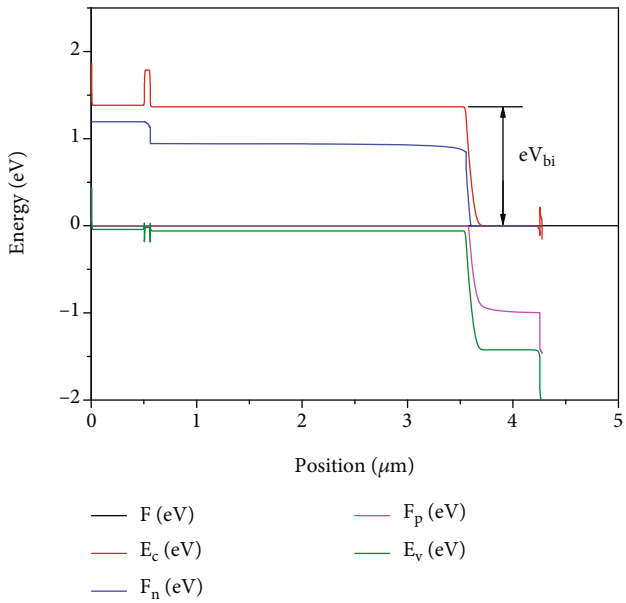

Figure 13: Energy band diagram of the GaAs-based solar cell under the AM1.5G spectrum. eV_{bi} represents the built-in voltage, which is also known as the built-in potential.

the charge carriers have a thermal energy distribution during almost all of their lifetime as a result of their collisions with the lattice [61].

3.8. Effect of Temperature on the Optimized Solar Cell. Since the solar cell is exposed to different climatic conditions, it is important and even necessary to study the evolution of the solar cell parameters at different operating temperatures. Thus, the performance of the solar cell depends on the temperature [62]. At higher operating temperature, the electron and hole mobility, carrier concentration, bandgap, and density of state are affected [63]. The influence of temperature on the performance parameters of the GaAs-based solar cell is studied for temperatures ranging from 10°C to 90°C. As can be seen in Figure 14, the V_{OC} (Figure 14(b)), FF (Figure 14(c)), and PCE (Figure 14(d)) decrease sharply with the increase in temperature, while the J_{SC} (Figure 14(a)) increases weakly with temperature due to the high recombination process that occurs at high temperatures [64, 65]. Thus, there is a decrease in V_{OC} from 1.2755 V to 1.2050 V, a decrease in FF from 89.70% to 87.00%, the PCE decreases from 36.0418% to 33.0530%, and finally, there is a slight increase in J_{SC} from 31.4987 mA/cm^2 to 31.5269 mA/cm^2.

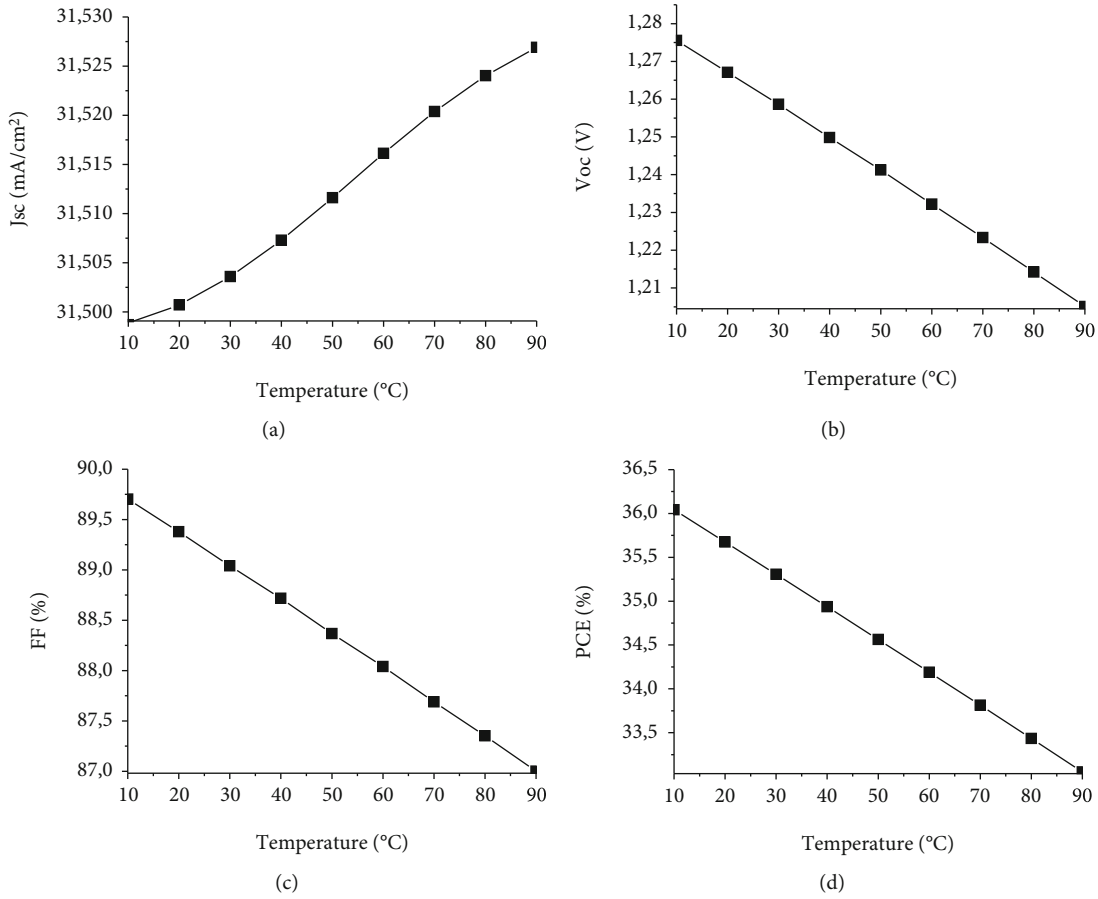

Figure 14: Effect of operating temperature on the electrical parameters of the GaAs-based solar cell: (a) J_{SC}, (b) V_{OC}, (c) FF, and (d) PCE.

We can also attribute the degradation of the performance of the solar cell to the fact that, at a high temperature, more electrons are released from the valence band to the conduction band; however, the electrons are volatile and move between the valence band and the conduction band. Therefore, in the absence of displacement motion, the recombination process will occur, which will cause the efficiency of the solar cell to decrease [66, 67].

4. Conclusion

In this work, we have simulated the performance of a homojunction GaAs solar cell in the Zn/n^+-$Al_xGa_{1-x}As$/n-GaAs/p-GaAs/p^+-$Ga_yIn_{1-y}P$(BSF)/p^+-GaAs/Mo configuration using the SCAP-1D software. We first investigated the influence of the proportions of aluminum (Al) and indium (In) in the window ($Al_xGa_{1-x}As$) and back surface field ($Ga_yIn_{1-y}P$) layers, respectively, on the solar cell performance. The results show that the $Al_{0.8}Ga_{0.2}As$/$Ga_{0.5}In_{0.5}P$ pair achieves better performance. Beyond these proportions ($x = 0.8$ and $y = 0.5$), the performance of the device degrades, mainly due to band offsets at the GaAs/AlGaAs and GaAs/GaInP interfaces (the donors thus spontaneously and irreversibly transfer their electrons into the low bandgap semiconductor). To emphasize the importance of the back surface field (BSF) layer, we compared the electrical parameters of the cell without and with the $Ga_{0.5}In_{0.5}P$ BSF layer. The presence of the $Ga_{0.5}In_{0.5}P$ BSF layer causes a significant improvement in the performance of the homojunction GaAs solar cell, with a power conversion efficiency of 32.19%. Subsequently, the performance of the obtained solar cell structure was analyzed as a function of different parameters (thickness, doping, and bulk defect density) of the p-GaAs base, n-GaAs emitter, and $Ga_{0.5}In_{0.5}P$ BSF layer. The power conversion efficiency of the solar cell increases with the emitter thickness. The recombination phenomenon is more pronounced than the electron-hole pair generation in the case of a thicker base. An increased presence of bulk defect density (above $10^{15}\,cm^{-3}$) in the absorber introduces new recombination centers that reduce the solar cell performance. A thin $Ga_{0.5}In_{0.5}P$ BSF layer reduces the carrier recombination rate at the back contact. The optimal values of $0.7\,\mu m$, $2\,\mu m$, and $0.55\,\mu m$ in thickness; $10^{17}\,cm^{-3}$, $10^{18}\,cm^{-3}$, and $5 \times 10^{18}\,cm^{-3}$ in doping; and $10^{15}\,cm^{-3}$, $10^{13}\,cm^{-3}$, and $10^{16}\,cm^{-3}$ in bulk defect density were obtained for the n-GaAs emitter, p-GaAs base, and $Ga_{0.5}In_{0.5}P$ BSF layer, respectively. The type of back contact material of the solar cell was also investigated in this work. It is found that increasing the back contact work function improves the performance of the solar cell due to the reduction of the Schottky barrier height and the recombination rate

at the back contact. The maximum efficiency is achieved with a platinum (Pt) electrode. Finally, the optimized GaAs-based solar cell in the Zn/n^+-$Al_{0.8}Ga_{0.2}As$/n-GaAs/p-GaAs/p^+-$Ga_{0.5}In_{0.5}P$(BSF)/p^+-GaAs/Pt configuration allowed us to obtain a short-circuit current density of 31.52 mA/cm^2, an open-circuit voltage of 1.26 V, a fill factor of 89.14%, and a power conversion efficiency of 35.44%. The effect of varying the operating temperature of the optimized GaAs-based solar cell allowed us to obtain a temperature coefficient of -0.036%/°C.

Data Availability

The simulation data used to support the findings of this study are included within the article.

Conflicts of Interest

The authors declare that there is no conflict of interest regarding the publication of this paper.

Authors' Contributions

C. Fotcha Kamdem provided substantial contributions to the conceptualization, methodology, software, writing the original draft, validation, and project administration. A. Teyou Ngoupo contributed to the conceptualization, methodology, software, writing the original draft, and validation. F. X. Abomo Abega and A. M. Ntouga Abena were assigned to the conceptualization, methodology, and software. J.-M. B. Ndjaka was responsible for the methodology, supervision, and validation.

Acknowledgments

The authors would like to extend their acknowledgment to Gent University, Belgium, for developing and providing the SCAPS-1D simulator used in this work.

References

[1] B. Arjunkumar, G. Ramalingam, M. Ramesh, J. S. Ponraj, and K. V. Rao, "Investigation of uni-directional nanorods composed microspheres and branched TiO_2 nanorods towards solar cell application," *Materials Letters*, vol. 273, article 127900, 2020.

[2] R. Perumalsamy, K. Kaviyarasu, S. Nivetha et al., "Preparation, characterization and structure prediction of In_2SnO_3 and spectroscopic (FT-IR, FT-Raman, NMR and UV-visible) study using computational approach," *Journal of Nanoscience and Nanotechnology*, vol. 19, no. 6, pp. 3511–3518, 2019.

[3] R. Vignesh, A. Muthuvinayagam, T. Elangovan, K. Kaviyarasu, G. T. Anand, and G. Ramalingam, "Unstable cell efficiency in CdS quantum dot sensitized solar cell using low cost lugols iodine aqueous electrolyte," *Materials Today: Proceedings*, vol. 36, pp. 159–162, 2021.

[4] K. C. Devendra, R. Wagle, R. Gaib, A. Shrivastava, and L. N. Mishra, "Modelling and simulation of AlGaAs/GaAs solar cell," *American Journal of Engineering Research*, vol. 9, no. 4, pp. 218–223, 2020.

[5] B. Li, X. B. Xiang, Z. P. You, Y. Xu, X. Y. Fei, and X. B. Liao, "High efficiency AlxGa1−xAsGaAs solar cells: Fabrication, irradiation and annealing effect," *Solar Energy Materials and Solar Cells*, vol. 44, no. 1, pp. 63–67, 1996.

[6] M. Hadrami, L. Roubi, M. Zazoui, and J. C. Bourgoin, "Relation between solar cell parameters and space degradation," *Solar Energy Materials and Solar Cells*, vol. 90, no. 10, pp. 1486–1497, 2006.

[7] J. Schön, G. M. Bissels, P. Mulder et al., "Improvements in ultra-light and flexible epitaxial lift-off GaInP/GaAs/GaInAs solar cells for space applications," *Progress in Photovoltaics: Research and Applications*, vol. 30, no. 8, pp. 1003–1011, 2022.

[8] D. K. Shah, K. C. Devendra, D. Parajuli, M. S. Akhtar, C. Y. Kim, and O. B. Yang, "A computational study of carrier lifetime, doping concentration, and thickness of window layer for GaAs solar cell based on Al_2O_3 antireflection layer," *Solar Energy*, vol. 234, pp. 330–337, 2022.

[9] S. C. Tsaur, A. G. Milnes, R. Sahai, and D. L. Feucht, "Theoretical and experimental results for GaAs solar cells," in *Proceedings of the Fourth International Symposium on GaAs and Related Compounds Conference Series, No. 17, The Institute of Physics*, p. 156, London, England, 1972.

[10] C. Hardingham and S. P. Wood, "High efficiency GaAs solar arrays in space," *GEC Review*, vol. 13, no. 3, pp. 163–171, 1998.

[11] J. J. Liou and W. W. Wong, "Comparison and optimization of the performance of Si and GaAs solar cells," *Solar Energy Materials and Solar Cells*, vol. 28, no. 1, pp. 9–28, 1992.

[12] A. Talhi, A. Belghachi, H. Moughli, B. Amiri, and L. Varani, "Numerical simulation of multi-quantum solar cells GaAs/InAs using Silvaco Atlas," *Digest Journal of Nanomaterials and Biostructures*, vol. 11, no. 4, pp. 1361–1366, 2016.

[13] H. Bourbaba, S. Kadri, and K. Djermane, "Optimization of the performance of GaAs solar cells: effect of the window layer," *Journal of Ovonic Research*, vol. 15, no. 3, pp. 151–156, 2019.

[14] K. C. Devendra, D. K. Shah, and A. Shrivastava, "Computational study on the performance of zinc selenide as window layer for efficient GaAs solar cell," *Materials Today: Proceedings*, vol. 49, pp. 2580–2583, 2022.

[15] D. van der Woude, L. van der Krabben, G. Bauhuis et al., "Ultrathin GaAs solar cells with a high surface roughness GaP layer for light- trapping application," *Progress in Photovoltaics: Research and Applications*, vol. 30, no. 6, pp. 622–631, 2022.

[16] C. F. Kamdem, A. T. Ngoupo, F. K. Konan, H. J. T. Nkuissi, B. Hartiti, and J. M. Ndjaka, "Study of the role of window layer Al0.8Ga0.2As on GaAs-based solar cells performance," *Indian Journal of Science and Technology*, vol. 12, no. 37, pp. 1–9, 2019.

[17] NREL, "Best research-cell efficiency chart," February 2023. https://www.nrel.gov/pv/cell-efficiency.html.

[18] M. Abderrezek, F. Djahli, M. Fathi, and M. Ayad, "Numerical modeling of GaAs solar cell performances," *Elektronika ir Elektrotechnika*, vol. 19, no. 8, pp. 41–44, 2013.

[19] B. Najat and D. Benmoussa, "Simulation and optimization performance of GaAs homojunction solar cell with BSF layer," in *2018 6th International Renewable and Sustainable Energy Conference (IRSEC)*, Rabat, Morocco, 2018.

[20] A. E. A. Saif, M. Albishri, A. Mindil, and M. Qaeed, "Superior efficiency for homojunction GaAs solar cell," *Journal of Ovonic Research*, vol. 19, no. 1, pp. 1–14, 2023.

[21] M. Burgelman, J. Verschraegen, S. Degrave, and P. Nollet, "Modeling thin-film PV devices," *Progress in Photovoltaics:*

Research and Applications, vol. 12, no. 23, pp. 143–153, 2004.

[22] M. Burgelman, P. Nollet, and S. Degrave, "Modelling polycrystalline semiconductor solar cells," *Thin Solid Films*, vol. 361-362, pp. 527–532, 2000.

[23] N. Khoshsirat and N. A. M. Yunus, "Numerical simulation of CIGS thin film solar cells using SCAPS-1D," in *2013 IEEE Conference on Sustainable Utilization and Development in Engineering and Technology (CSUDET)*, Selangor, Malaysia, 2013.

[24] H. Movla, "Optimization of the CIGS based thin film solar cells: numerical simulation and analysis," *Optik*, vol. 125, no. 1, pp. 67–70, 2014.

[25] M. Burgelman, K. Decock, A. Niemegeers, J. Verschraegen, and S. Degrave, *The SCAPS-1D Software*, University of Gent, Department of Electronics and Information Systems (ELIS), Belgium, 2018.

[26] M. Powalla, P. Jackson, W. Witte et al., "High-efficiency $Cu(In,Ga)Se_2$ cells and modules," *Solar Energy Materials and Solar Cells*, vol. 119, pp. 51–58, 2013.

[27] L. Atourki, H. Kirou, A. Ihlal, and K. Bouabid, "Numerical study of thin films CIGS bilayer solar cells using SCAPS," *Materials Today: Proceedings*, vol. 3, no. 7, pp. 2570–2577, 2016.

[28] A. W. Haas, J. R. Wilcox, J. L. Gray, and R. J. Schwartz, "Design of a GaInP/GaAs tandem solar cell for maximum daily, monthly, and yearly energy output," *Journal of Photonics for Energy*, vol. 1, no. 1, article 018001, 2011.

[29] N. Messei and M. S. Aida, "Numerical simulation of front graded and fully graded AlGaAs/GaAs solar cell," *Optik*, vol. 126, no. 23, pp. 4432–4435, 2015.

[30] A. McEvoy, T. Markvart, and L. Castaner, *Practical Handbook of Photovoltaics Fundamentals and Applications*, Elsevier Ltd, 2nd Ed. edition, 2012.

[31] Y. Zhao, J. S. Xue, J. C. Zhang, X. W. Zhou, Y. C. Zhang, and Y. Hao, "InAlN/InGaN/GaN double heterostructure with improved carrier confinement and high-temperature transport performance grown by metal-organic chemical vapor deposition," *Semiconductor Science and Technology*, vol. 30, no. 7, article 075005, 2015.

[32] T. Kehagias, N. Florini, J. Kioseoglou et al., "Nanostructure and strain properties of core-shell GaAs/AlGaAs nanowires," *Semiconductor Science and Technology*, vol. 30, no. 11, article 114012, 2015.

[33] C. Grasse, G. Boehm, M. Mueller, T. Gruendl, R. Meyer, and M. C. Amann, "Empirical modeling of the refractive index for (AlGaIn) as lattice matched to InP," *Semiconductor Science and Technology*, vol. 25, no. 4, article 045018, 2010.

[34] Y. A. Goldberg, "Aluminium gallium arsenide (Al(x)Ga(1-x)as)," in *Handbook Series on Semiconductor Parameters. Volume 2*, pp. 1–36, World Scientific Publishing Co., Singapore, 1999.

[35] P. Würfel, *Physics of Solar Cells: From Principles to New Concepts*, Wiley vch Verlag GmbH & Co, KGaA, 2005.

[36] M. S. Salem, O. M. Saif, A. Shaker et al., "Performance optimization of the InGaP/GaAs dual-junction solar cell using SILVACO TCAD," *International Journal of Photoenergy*, vol. 2021, Article ID 8842975, 12 pages, 2021.

[37] J. M. Olson, D. J. Friedman, and S. Kurtz, "High-efficiency III-V multijunction solar cells," in *Handbook of Photovoltaic Science and Engineering*, pp. 359–411, John Wiley & Sons, Ltd, 2003.

[38] M. Verma, S. R. Routray, and G. P. Mishra, "Analysis and optimization of BSF layer for highly efficient GaInP single junction solar cell," *Materials Today: Proceedings*, vol. 43, pp. 3420–3423, 2021.

[39] J. Verma, P. Dey, A. Prajapati, and T. D. Das, "Multi BSF Layer InGaP/GaAs optimized solar cell," in *2016 International Conference on Microelectronics, Computing and Communications (MicroCom)*, Durgapur, India, 2016.

[40] A. D. Khan, A. D. Khan, S. D. Khan, and M. Noman, "Light absorption enhancement in tri-layered composite metasurface absorber for solar cell applications," *Optical Materials*, vol. 84, pp. 195–198, 2018.

[41] A. N. Abena, A. T. Ngoupo, and J. M. B. Ndjaka, "Computational analysis of mixed cation mixed halide-based perovskite solar cell using SCAPS-1D software," *Heliyon*, vol. 8, no. 11, article e11428, 2022.

[42] M. S. Chowdhury, S. A. Shahahmadi, P. Chelvanathan et al., "Effect of deep-level defect density of the absorber layer and n/i interface in perovskite solar cells by SCAPS-1D," *Results in Physics*, vol. 16, article 102839, 2020.

[43] D. M. Caughey and R. E. Thomas, "Carrier mobilities in silicon empirically related to doping and field," *Proceedings of the IEEE*, vol. 55, no. 12, pp. 2192-2193, 1967.

[44] A. Toshniwal, A. Jariwala, V. Kheraj, A. S. Opanasyuk, and C. J. Panchal, "Numerical simulation of tin based perovskite solar cell: effects of absorber parameters and hole transport materials," *Journal of Nano-and Electronic Physics*, vol. 9, no. 3, article 03038, 2017.

[45] M. I. Kabir, Z. Ibrahim, K. Sopian, and N. Amin, "Effect of structural variations in amorphous silicon based single and multijunction solar cells from numerical analysis," *Solar Energy Materials and Solar Cells*, vol. 94, no. 9, pp. 1542–1545, 2010.

[46] A. Fantoni, M. Viera, and R. Martins, "Influence of the intrinsic layer characteristics on a-Si:H p-i-n solar cell performance analysed by means of a computer simulation," *Solar Energy Materials and Solar Cells*, vol. 73, no. 2, pp. 151–162, 2002.

[47] G. Wlérick, "Équilibre électronique d'un semi-conducteur éclair é," *Journal de Physique et le Radium*, vol. 15, no. 10, pp. 667–676, 1954.

[48] A. Cho and N. Park, "Impact of interfacial layers in perovskite solar cells," *ChemSusChem*, vol. 10, no. 19, pp. 3687–3704, 2017.

[49] H. R. Arzbin and A. Ghadimi, "Improving the performance of a multi-junction solar cell by optimizing BSF, base and emitter layers," *Materials Science and Engineering B*, vol. 243, pp. 108–114, 2019.

[50] P. Pandey, A. Bhatnagar, and V. Janyani, "Multi-junction solar cell based on efficient III–V InGaP/GaAs with GaInAsP as BSF layers," in *Optical and Wireless Technologies*, V. Janyani, G. Singh, M. Tiwari, and A. d'Alessandro, Eds., Springer, Singapore, 2020.

[51] A. E. Benzetta, M. Abderrezek, and M. E. Djeghlal, "Comparative study on $Cu_2ZnSn(S,Se)_4$ based thin film solar cell performances by adding various back surface field (BSF) layers," *Chinese Journal of Physics*, vol. 63, pp. 231–239, 2020.

[52] M. M. A. Moon, M. H. Ali, M. F. Rahman, A. Kuddus, J. Hossain, and A. B. M. Ismail, "Investigation of thin-*p*-$BaSi_2$/n-CdS heterostructure towards semiconducting silicide based high efficiency solar cell," *Physica Scripta*, vol. 95, no. 3, article 035506, 2020.

[53] M. P. Godlewski, C. R. Baraona, and H. W. Brandhorst Jr., "Low-high junction theory applied to solar cells," *Solar Cells*, vol. 29, no. 2-3, pp. 131–150, 1990.

[54] O. K. Simya, A. Mahaboobbatcha, and K. Balachander, "Compositional grading of CZTSSe alloy using exponential and uniform grading laws in SCAPS-ID simulation," *Superlattices and Microstructures*, vol. 92, pp. 285–293, 2016.

[55] M. Thambidurai, S. Foo, K. M. Salim et al., "Improved photovoltaic performance of triple-cation mixed-halide perovskite solar cells with binary trivalent metals incorporated into the titanium dioxide electron transport layer," *Journal of Materials Chemistry C*, vol. 7, no. 17, pp. 5028–5036, 2019.

[56] H. B. Michaelson, "The work function of the elements and its periodicity," *Journal of Applied Physics*, vol. 48, no. 11, pp. 4729–4733, 1977.

[57] J. Hölzl and F. K. Schulte, "Work function of metals," in *Solid Surface Physics*, vol. 85, pp. 1–150, Springer, Berlin, Heidelberg, 1979.

[58] S. M. Thahab, H. A. Hassan, and Z. Hassan, "Effects of metal work function and operating temperatures on the electrical properties of contacts to n-type GaN," in *2006 IEEE International Conference on Semiconductor Electronics*, Kuala Lumpur, Malaysia, 2006.

[59] M. S. Rana, M. M. Islam, and M. Julkarnain, "Enhancement in efficiency of CZTS solar cell by using CZTSe BSF layer," *Solar Energy*, vol. 226, pp. 272–287, 2021.

[60] K. Attari, L. Amhaimar, A. Asselman, and M. Bassou, "The design and optimization of GaAs single solar cells using the genetic algorithm and Silvaco ATLAS," *International Journal of Photoenergy*, vol. 2017, Article ID 8269358, 7 pages, 2017.

[61] S. N. F. Mott and R. W. Gurney, "Electronic processes in ionic crystals," Clarendon Press, New York: Oxford, 2nd ed. edition, 1948.

[62] N. Papageorgiou, Y. Athanassov, M. Armand et al., "The performance and stability of ambient temperature molten salts for solar cell applications," *Journal of the Electrochemical Society*, vol. 143, no. 10, pp. 3099–3108, 1996.

[63] A. Mesrane, F. Rahmoune, A. Mahrane, and A. Oulebsir, "Design and simulation of InGaN - junction solar cell," *International Journal of Photoenergy*, vol. 2015, Article ID 594858, 9 pages, 2015.

[64] A. Mahfoud, F. Mohamed, S. Mekhilef, and F. Djahli, "Effect of temperature on the GaInP/GaAs tandem solar cell performances," *International Journal of Renewable Energy Research*, vol. 5, no. 2, pp. 629–634, 2015.

[65] A. R. Jha, *Solar Cell Technology and Applications*, Auerbach Publications, New York, 2009.

[66] A. O. Maka and T. S. O'Donovan, "Effect of thermal load on performance parameters of solar concentrating photovoltaic: high-efficiency solar cells," *Energy and Built Environment*, vol. 3, no. 2, pp. 201–209, 2022.

[67] Y. P. Varshni, "Temperature dependence of the energy gap in semiconductors," *Physica*, vol. 34, no. 1, pp. 149–154, 1967.